The Astrophysical Journal, 693:1500–1507, 2009 March 10 doi:10.1088/0004-637X/693/2/1500

OBSERVATIONS OF MAIN-SEQUENCE STARS AND LIMITS ON EXOZODICAL DUST WITH NULLING INTERFEROMETRY*

Wilson M. Liu, Philip M. Hinz, William F. Hoffmann, Guido Brusa, Doug Miller, and Matthew A. Kenworthy
Steward Observatory, University of Arizona, 933 North Cherry Avenue, Tucson, AZ 85721, USA; wliu@as.arizona.edu
Received 2007 December 20; accepted 2008 December 8; published 2009 March 9

ABSTRACT

We present nulling interferometric observations of six nearby main-sequence stars (α CrB, α Lyr, β Leo, γ Ser, ϵ Eri, and ζ Lep). None of the stars show evidence for a positive detection of warm debris in the habitable zone of the systems. Using a scaled up model of solar zodiacal emission, the 3σ upper limits on dust density range from 220 to 10^4 Zody (1 Zody = the density of our own solar zodiacal cloud) depending on the particular star, corresponding to mass limits of 10^{-7} to 10^{-5} $M_\oplus$ of micron-sized dust. These limits contrast with the presence of dust at greater separations from the star, implying a clearing in dust in the inner system. This suggests that the inner circumstellar environment around nearby intermediate-mass main-sequence stars more than several tens of millions of years old are generally cleared of dusty debris. Finally, the well studied nature of the debris disks around Vega, ϵ Eridani, and ζ Leporis allows us to place these 10 μm nulling observations in the context of previous studies to determine the physical processes responsible for shaping the debris disk in these particular systems.

Key words: circumstellar matter – instrumentation: adaptive optics – stars: individual (α CrB, α Lyr, β Leo, γ Ser, ϵ Eri, ζ Lep) – techniques: interferometric

1. INTRODUCTION

As intermediate-mass stars evolve onto the main sequence, they shed their natal gas-rich disks. The material that remains around mature main-sequence stars is often referred to as a "debris disk," which is gas poor and composed of solid dust particles. These "second generation" debris disks are necessarily shaped and changed over time by internal interactions as well as interactions with planetary bodies, and can thus be a powerful tool in determining the structure and evolution of planetary systems.

Solid debris surrounding a main-sequence star can be observed at a range of wavelengths, each probing a different spatial scale, with longer wavelengths probing greater separations from the parent star. Warm dust ($T > 300$ K) in the inner system (separations of a few AU or less) can be observed through thermal emission at wavelengths shortward of 10 μm. This debris is analogous to the zodical dust in our own system; a population of grains which is generated through steady-state collisional processes in the Main Belt of asteroids, and exist for relatively long timescales. Hot dust can also be generated by stochastic events, such as a large collision or series of collisions analogous the Moon forming collision and Late Heavy Bombardment phase of our solar system. Such an event has been used to explain the presence of small grains detected around Vega by the *Spitzer Space Telescope* (Su et al. 2005).

Although many cases of cold dust at far-IR wavelengths (i.e., analogous to the Kuiper Belt in our own solar system) have been confirmed, to date there have been relatively few spatially resolved detections of emission at 10 μm surrounding main-sequence stars. Whether this is a result of a need for greater sensitivity and/or spatial resolution in the observations, or due to a physical reason in the observed systems is not certain. There are a number of systems currently known to have strong mid-IR excesses, including ζ Leporis (e.g., Chen & Jura 2001) and β Pictoris (e.g., Backman & Paresce 1993), which may suggest the presence of warm dust in the terrestrial planet-forming zones. Recently, observational studies, including those of Smith et al. (2008) and Uzpen et al. (2005) have identified several main-sequence stars which may possess terrestrial zone debris. However, spatially resolved observations of such disks is challenging. We investigate several of these systems by using nulling interferometry to achieve improved spatial resolution and the contrast necessary to begin probing whether warm debris is present in nearby main-sequence systems. A detection would be evidence for the existence of warm (300 K) dust close to the star, located in the habitable zone of the system.

Nulling interferometry is a technique used to study spatially resolved circumstellar material in the presence of unresolved flux, and represents an ideal opportunity to observe the circumstellar environments of main-sequence stars. The technique, first proposed by Bracewell (1978) is implemented by overlapping the pupils of two telescopes (or two subapertures on a single-aperture telescope) with an optical path length difference of one-half λ between the beams. The result of such a configuration is a sinusoidal transmission function with the functional form

$$T(\theta) = \sin^2(\pi b\theta/\lambda), \quad (1)$$

where b is the baseline of the interferometer, λ is the wavelength of observations, and θ is the angular distance from the observed object to the pointing center of the interferometer (Hinz et al. 1998). During observations, the central destructive fringe is placed on the unresolved point source. This allows us to detect spatially resolved emission, effectively isolating it from the unresolved stellar flux. Nulling interferometry provides the necessary contrast to observe faint circumstellar material in the presence of a much brighter star, currently achieving contrast ratios of about 100. A large contrast ratio is essential when observing debris disks surrounding main-sequence stars, where stellar flux outshines the debris, usually by at least a factor of several hundreds. This technique can detect material as close to the star as one-quarter of the fringe spacing where the light is neither suppressed nor enhanced. This corresponds to 0.″12 for the configuration used on the MMT, or 12 AU about a star at

* The results presented here made use of the MMT Observatory, a jointly operated facility of the University of Arizona and the Smithsonian Institution.

100 pc. This is between 2 and 3 times finer than the diffraction limit of the 6.5 m primary at the wavelengths observed (8–13 μm). The outer working angle (i.e., outermost separation probed by the observation) is determined by the size of the aperture used in photometry, described in Section 2.

In this paper, we present the results of nulling interferometric observations of main-sequence stars with nulling interferometry. We present the observations in Section 2 and discuss results in Sections 3 and 4. We summarize our findings in Section 5.

2. OBSERVATIONS AND DATA REDUCTION

2.1. Target Selection

The targets observed in this study were chosen to maximize the chances of spatially resolving a warm debris disk, as well as to take advantage of previous observations of the objects at different wavelengths (i.e., our high spatial resolution 10 μm observations will complement observations that already exist in the literature). Five of the six objects are intrinsically luminous (A- or F-type), so that the circumstellar debris will be heated out to a large radius. Assuming a blackbody grain temperature law of $T_g = 278 L_*^{1/4} r_{\rm AU}^{-1/2}$ (Backman & Paresce 1993), the habitable zone should lie at separations ranging from 4 to 7 AU (for the A stars). Objects within 40 pc are chosen for the same reason (ability to spatially resolve the emission), and all objects have 10 μm fluxes greater than 1 Jy to ensure sensitivity to the object. Finally, each of the A-type stars has a 24 μm excess detected by *Spitzer* (Rieke et al. 2005), which make them ideal candidates for 10 μm observations to complement the longer wavelength observations, thus giving a more complete picture of the circumstellar dust at different spatial scales. Also included in the target list is the K-type star ϵ Eri. The star lies at a distance of 3 pc, making a hypothetical 10 μm disk around the star resolvable. Previous studies have found that the star has 25, 60, and 100 μm excess detected by *IRAS* (Backman & Paresce 1993; Silverstone 2000). The final target, γ Ser, has no detected 25 μm excess, but does have a 60 μm excess detected by *IRAS* (Backman & Paresce 1993).

The complete list of targets is shown in Table 1 along with their stellar parameters and 24 μm excess ratios, where available.

Table 1
Main-Sequence Target List

Name	Alt. Name	Spec. Type[a]	d (pc)[b]	Est. Ages (Myr)	24 μm Excess Ratio	Refs.[c]
α CrB	Alphecca, HD 139006	A0	23	350	1.29	1, 2, 3
α Lyr	Vega, HD 172167	A0	7.8	365	1.15	1, 2, 3
β Leo	Denebola, HD 102647	A3	12	50, 520	1.42	1, 2, 3
γ Ser	HD 142860	F6	11	1600, 3200	...	1, 2, 4
ϵ Eri	HD 22049	K2	3.2	800	1.12	1, 2, 5
ζ Lep	HD 38678	A2	22	180, 231, 330	2.43	1, 2, 3, 4

Notes. [a] Spectral type; [b] distance; [c] age references.
References. 1. SIMBAD; 2. Perryman et al. (1997); 3. Rieke et al. (2005) and references therein; 4. Chen et al. (2006) and references therein; 5. Benedict et al. (2006) and references therein.

2.2. Observations and Calculating the Null

Observations of the six main-sequence targets were made between 2003 May and 2006 June at the MMT 6.5 m telescope. All observations of these objects made use of the MMT adaptive optics (MMTAO) system, which uses a deformable secondary mirror. Since the secondary mirror of the telescope *is* the deformable mirror, there is no need for an intermediate set of correcting optics between the telescope and science camera. This reduces the number of warm surfaces in the optical path, minimizing background and maximizing throughput. Conventional AO systems typically have a background emissivity of about 20%, compared to a deformable secondary system which can have emissivities in the range of 5%–7%. This can translate to a 3–4 times speed improvement in mid-IR observations. More technical details regarding the MMT adaptive secondary can be found in Brusa et al. (2003).

MMTAO also provides additional benefits when used concurrently with nulling interferometry. First, wave front aberrations introduced by the atmosphere that might affect the suppression level of the null are significantly reduced or eliminated. This allows one to precisely tune the path length between the arms of the interferometer for the best possible contrast ratio. The addition of wave front correction also lessens the amplitude of phase variations from frame to frame, resulting in smaller errors in calibration. The configuration and setup of the BLINC-MIRAC instrument were otherwise identical to observations described in previous papers (Liu et al. 2005, 2004). Images were taken in the N band (10.6 μm, 50% bandpass). Due to the increased stability in null afforded by AO, integrations were generally 1 s per frame (compared to the 50 ms frames needed to "freeze out" seeing effects for non-AO observations). An integration of 1 s results in a 3σ detection of a 1.5 Jy source. We take three sets of 10 frames (a total of 30 s integration) on the object with the interferometer tuned to destructive interference, followed by 10 frames of the object in constructive interference. After three repetitions of this sequence, a set of 10 off-source frames for sky subtraction is taken with the same integration time per frame as the on-source images. This procedure is repeated as many times as possible for both science objects and point-source (spatially unresolved) calibrator stars. From the destructively and constructively interfered images, aperture photometry is extracted. The aperture size is set to the point at which the signal from the star disappears into the background noise. This also determines the outer working angle of the observations. Using the photometry, we calculate the *instrumental null* which is defined as

$$N = \mathrm{Flux}_{\mathrm{nulled}}/\mathrm{Flux}_{\mathrm{constructive}} \quad (2)$$

and expressed as a percent. The instrumental null is calculated for both the science and calibrator stars. The difference between the instrumental null of the science object and the calibrator is called the *source null*. The source null represents the spatially resolved flux around the science object as a percentage of its full flux. A source null of zero means that the science object is spatially unresolved. Table 2 lists the dates, number of nulled frames, and the range of separations probed for each object.

Except for Vega which has a 10 μm flux in excess of 40 Jy, the objects were faint enough that the image of the object dropped below the noise level in the frames when destructively interfered, making photometry impossible. For this reason, we used a combination of techniques in order to assess an upper limit on the instrumental null for the five objects in question. The

Table 2
Main-Sequence Summary of Observations

Star	Dates	No. of Destructive Frames	Inner (AU)	Outer (AU)
α CrB	2005 Jun 26	60	2.8	26
α Lyr	2003 May 10–12	140	0.9	6
β Leo	2005 Jun 26, 2006 Feb 11	660	1.4	13
γ Ser	2006 Jun 17–18	150	1.3	5
ϵ Eri	2006 Feb 11	150	0.4	3
ζ Lep	2006 Feb 11	30	2.6	19

Table 3
Main-Sequence Nulls

Name	Date	Method[a]	Instrumental Null (%)	Callibator 1 Null[b]	Callibator 2 Null	Source Null
α CrB	2005 Jun	S	15 ± 4	6.2 ± 0.1	N/A	8.8 ± 4
"	2005 Jun	E	10 ± 4	6.2 ± 0.1	N/A	4 ± 4
α Lyr	2003 May	N	3.7 ± 0.7	3.6 ± 0.5	3.4 ± 0.4	0.2 ± 0.7
β Leo	2006 Feb	N	4.6 ± 2.3	5.8 ± 0.7	4.9 ± 0.8	-0.8 ± 2.4
"	2006 Jun	S	4.0 ± 1.2	3.6 ± 0.4	3.4 ± 0.4	0.5 ± 1.3
γ Ser	2006 Jun	A	5.9 ± 2.6	2.8 ± 0.1	4.6 ± 0.2	2.2 ± 2.6
ϵ Eri	2006 Feb	A	3 ± 2	4.5 ± 0.4	3.5 ± 0.5	-1 ± 2
"	2006 Feb	E	6 ± 2	4.5 ± 0.4	3.5 ± 0.5	2 ± 2
ζ Lep	2006 Feb	A	10 ± 5	3.5 ± 0.5	4.6 ± 0.3	6 ± 6

Notes.
[a] N: normal reduction procedure; A: artificial star tests; S: stacked frames; E: signal-to-noise estimate.
[b] All calibrator nulls assessed using normal reduction procedure. Cal. 1 data were taken before the science object, Cal. 2 were taken after.

first technique used to estimate the upper limit on the null was a series of artificial star tests. Artificial stars were created using the constructively interfered images of the object and scaled to a percentage of the full flux. The artificial star was then added to the data frame, to see if the star was detectable over the noise of the frame. This was repeated for artificial stars of increasing flux until the level of the noise could be assessed. For those stars for which there were a large number of frames taken, we stacked the frames in order to improve the signal-to-noise ratio (S/N). In some cases, this allowed us to estimate an instrumental null for the object. Finally, we used the signal-to-noise in the constructively interfered frame to estimate the null that would be detectable in a destructive frame (i.e., if the full flux frame has an S/N of 10, we estimate that any null greater than 10% would be measurable). The latter is the least accurate and precise of all the techniques used and provides only a very rough estimate of the upper limit on the instrumental null. Table 3 shows the instrumental and source nulls achieved for each object (science and calibrator), along with the method used to assess the null.

For the objects in this sample, the noise level becomes significant, thus the precision of photometry is affected. Improvements in wave front correction with AO has also decreased phase variation, making the photometric error the larger contributor to the error in many cases. A typical example of error contributions is seen in the observations of γ Ser, which has a error in source null of $\pm 2.6\%$. This value is derived by adding in quadrature the contributions from the photometric error ($\pm 2.2\%$) and the phase variation ($\pm 1.4\%$).

3. RESULTS FROM THE FULL SAMPLE

In this section, we interpret the upper limits for the source nulls with a physical model. Three models are used, including a scaled solar zodiacal dust cloud, a zodiacal disk with a several AU-sized inner clearing, and a more general optically thin dust disk. These models all assume steady-state disks. Stochastic processes in the systems could have significant effects on the dust densities and distribution in these systems, leading to an increase of several orders of magnitude density, as well as large spatial distributions for small grains ejected by radiation pressure (tens to hundreds of AU around A-type stars) as seen in observations of Vega (Su et al. 2005). We do not consider these stochastic events in this section but discuss them in the context of individual objects in Section 4.

3.1. A Scaled Solar Zodiacal Dust Cloud

The source nulls for all six objects show no spatially resolved circumstellar emission. The upper limits in the source nulls represent different upper limits for warm habitable zone dust density in each system. In order to assess these dust density limits, we use a scaled solar zodiacal dust model based upon Kelsall et al. (1998).

The Kelsall et al. (1998) zodiacal dust model incorporates several components to model our solar system's inner dust, including a "smooth cloud" component as well as several dusty asteroid rings. For the purpose of this analysis we consider only the smooth cloud component, which dominates the detectable dust. This component is an optically thin cloud with a power-law fall-off in density with increasing separation from the star and a dependence of $r^{-1.3}$. Additionally, the cloud has a vertical density profile which decreases exponentially with increasing height from the midplane (Kelsall et al. 1998, Equations 6 and 7). For our model, we set the inner boundary of the cloud at the dust sublimation radius and the outer boundary at 10 AU, outside the 10 μm emitting region for our objects.

This model was used to predict the flux from an exozodiacal cloud surrounding each star and convolved with the transmission function of the nulling interferometer in order to simulate the observed null. Stellar parameters (e.g., M_*, R_*, L_*) adopted for each star were taken to be the typical values for each spectral type, as listed in Cox (2000). Values for the stellar fluxes were adopted to be the color-corrected *IRAS* 12 μm fluxes (Backman & Paresce 1993). The density of the exozodiacal cloud in the model was varied in order to match the output to the actual observed nulls. For the upper limits in source null we use a 3σ limit; for stars with more than one method used for deriving the null, we use the larger of the two errors. Once a limit on the density was calculated for each star, this was converted to a dust mass. The density limit for each star was converted to an effective emitting area using a value for the solar zodiacal cloud of 1 Zody $\approx 10^{21}$ cm^2 multiplied by the factor for the density limit determined using the Kelsall et al. (1998) model described above. For the size distribution of grains, we adopt a power-law dependence of

$$n(a)da = n_o a^{-p}, \quad (3)$$

where n is the number of grains of a given radius a, and p is 3.5 (Mathis et al. 1977; Greenberg & Nolan 1989). The lower limit for grain size was taken to be the blowout size for grains surrounding the A-type stars (Artymowicz 1988),

$$a_{\min} = 3L_* Q_{\rm pr}/16\pi M_* c\rho, \quad (4)$$

where $Q_{\rm pr} \approx 1$ and ρ is the density of grain material, taken to be 2.5 g cm^{-3} (Grun et al. 1985). For the later type stars, the minimum grain size was taken to be 1 μm to provide a

Table 4
Derived Limits on Dust Properties Using a Scaled Zody Model

Name	Null Limit (%)	Density (Zody)	Surf. Area (cm^2)	a_{min} (μm)	Mass[a] ($M_\oplus$)	f_d
α CrB	12	6.4×10^3	6.4×10^{24}	4.3	2.9×10^{-5}	6.4×10^{-4}
α Lyr	2.1	2.2×10^2	2.2×10^{23}	4.3	9.7×10^{-7}	2.2×10^{-5}
β Leo	7.2	1.0×10^3	1.0×10^{24}	1.9	5.9×10^{-7}	1.0×10^{-4}
γ Ser	7.8	6.0×10^3	6.0×10^{24}	1.0	2.6×10^{-6}	6.0×10^{-4}
ϵ Eri	6.0	6.5×10^3	6.5×10^{24}	1.0	2.9×10^{-6}	6.5×10^{-4}
ζ Lep	18	9.0×10^3	9.0×10^{24}	1.8	5.3×10^{-6}	9.0×10^{-4}

Note.
[a] Grains ranging in size from blowout size to 1 mm, assuming the dust lies between the dust sublimation radius and 10 AU.

conservative estimate of the upper limit for dust mass. The maximum grain size used in the calculation of dust mass was 1000 μm. Thus, the masses derived can be considered as the upper limit for the total mass found in grains smaller than 1 mm. The derived values for the total disk mass depend on the largest size of grain (or planetesimal) considered. If the size of the largest object is increased by a factor of 10^6 to 1 km; the total mass will increase by a factor of about 10^3. The total emitting surface area remains roughly the same. In other words, the total surface area of debris is dominated by small grains, but the total mass is dominated by the largest bodies. Values for the dust density, blowout size, and dust mass can be found in Table 4. We find the 3σ source null upper limits generally correspond to densities of 10^3 to 10^4 Zody and dust masses on the order of $10^{-6}\ M_\oplus$.

In addition, we estimate the limit for fractional dust luminosity $f_d = L_{\rm dust}/L_*$ by assuming 1 Zody $= 10^{-7}$ in f_d (Beichman et al. 2005). These values are also listed in Table 4, and the values are on the order of $f_d \sim 10^{-4}$.

A further analysis can be made by comparing the observed limits on dust to an estimate of the expected density of our own zodiacal dust *at the age of each observed star*. In this way we can compare "apples to apples" with regard to stellar age. For a collisionally replenished disk with a dust removal timescale much shorter than the lifetime of the system, we expect $f_d \sim t^{-2}$ for a Poynting–Robertson (P–R) drag dominated disk (Spangler et al. 2001). Using this relation we find that the density of solar system zodiacal dust at the age of Vega (365 Myr), for example, would be 150 Zody. Our limit of 220 Zody results in a limit on warm dust in the Vega system of about 1.5 times our own zodiacal dust, after accounting for dust evolution. If the fractional dust luminosity follows a evolutionary trend of $f_d \sim t^{-1}$ for a disk dominated by collisional removal of grains as predicted in Dominik & Decin (2003), we would expect a dust limit of about 41 times solar. Table 5 shows the density of dust in each system as a factor of solar level, after accounting for dust evolution. For stars with multiple age determinations, an average was used.

As mentioned above in the description of the target-selection criteria, all targets have excesses detected at longer wavelengths by previous studies. The amounts of long wavelength dust emission varies across the sample. The A-stars in the sample all had fairly large 24 μm excesses, reported in Rieke et al. (2005), of 29%, 15%, 42%, and 143% above the stellar photospheric level, for α CrB, α Lyr, β Leo, and ζ Lep, respectively. If these same excesses were present at 10 μm, they would have been easily detected with our nulling observations. Since this is not the case, we can infer that these systems are relatively clear of the material in the inner system (i.e., a few AU in separation) compared to larger radii. A further discussion of the well-studied debris disks around Vega and ζ Lep is contained in the following sections. The star γ Ser is somewhat puzzling, as it had an significant excess at 60 μm detected by *IRAS*, with no excess at 25 or 100 μm. However, recent Multiband Imaging Photometer for *Spitzer* (MIPS) observations at 70 μm failed to find any excess emission. Additionally, *Spitzer* IRS observations show no excess between 5 and 35 μm (Chen et al. 2006). These results suggest that the positive detection by *IRAS* were due to confusion from its large beam size. If this is the case, then it would point toward the γ Ser system to be devoid of solid debris at a range of spatial scales, from a few to hundreds of AU. Finally, ϵ Eri has a well established debris disk detected at submillimeter wavelengths containing a large quantity of material (several earth masses) at radii of tens of AU. Again, this implies the existence of a clearing process keeping the inner system relatively devoid of material. We examine this star in depth in Section 4.

Table 5
Evolution-Adjusted Dust Limits (Multiples of Solar Level)

Name	$f_d \sim t^{-2}$	$f_d \sim t^{-1}$
α CrB	73	930
α Lyr	3.3	41
β Leo	6.8	110
γ Ser	4.3×10^3	8.0×10^3
ϵ Eri	240	1.3×10^3
ζ Lep	56	1.1×10^3

3.2. Size of the Inner Clearing

To assess the physical scale of the inner clearing in the five systems with confirmed excess at longer wavelengths, we again use an optically thin, scaled solar zodiacal dust model based on Kelsall et al. (1998). The model is scaled up to a density which corresponds to the positive detection of excess at longer wavelengths. For the four A-stars, this is the excess reported in Rieke et al. (2005) for 24 μm emission. For ϵ Eri, we adopt the 25 μm excess detected by *IRAS*. We then introduce an artificial inner edge to the disk (replacing the dust sublimation radius) and vary the radius of the inner edge to match the detection limit of the nulling observations. For the purposes of this analysis, the outer radius of the disk is set to 80 AU, roughly 2–3 times the radius at which one would expect the 24 μm to peak for the A-stars. This is very likely to be an oversimplified model, and does not apply well to ζ Lep which has a known 10 μm excess that either falls below the detection threshold or under the spatial resolution limit of our observations. However, this analysis does gives us an idea of the physical scale for the (minimum) inner clearing sizes in these systems, should an inner clearing be responsible for the lack of a positive detection. The values of the derived inner gap radius for each star are listed in Table 6 and can be interpreted as a minimum value. The source null derived using the model is fairly sensitive to changes in the inner hole size. As a typical example, changing the hole size of the β Leo disk by $\pm 10\%$ results in a range of source nulls between and 5.5% and 10.3%, corresponding to a 2σ error in the null.

3.3. A General Optically Thin Disk

Finally, a more general treatment of an optically thin disk can be made, following the model of Mamajek et al. (2002), which incorporates spherical grains of a single size, $\langle a \rangle = 5a_{\rm min}/3$, which represents an average size for the power-law

Table 6
Derived Inner Gap Sizes

Name	Excess Ratio[a]	Min. $r_{\rm hole}$ (AU)
α CrB	1.29	13
α Lyr	1.15	13
β Leo	1.42	12
ϵ Eri	1.12	2.5
ζ Lep	2.43	26

Note.
[a] 24 μm excess detected by *Spitzer* and reported by (Rieke et al. 2005), except for ϵ Eri which uses the 25 μm excess measured by *IRAS* and reported in Backman & Paresce (1993).

size distribution described above. The grains lie in an annular distribution from the dust sublimation radius out to a radius where there is no longer significant 10 μm emission (about 25 AU for A-type stars). The derived parameters for dust mass and fractional dust luminosity are shown in Table 7, and generally agree to within an order of magnitude of the levels of dust found using a scaled zodiacal disk model above.

The lack of warm debris in the main-sequence sample is perhaps not surprising, in light of recent observational and theoretical results. A recent *N*-band photometric survey of 14 T Tauri stars in the Tucana–Horologium association finds that none has a significant excess (Mamajek et al. 2004). Assuming an optically thin disk, this constrains the mass in the inner 10 AU of these systems to less than 10^{-6} $M_{\oplus}$, similar to the mass limits established for the sample in this study. As the Tuc–Hor stars have lower masses than many of the objects in the nulling sample presented in this paper, this appears to be evidence that debris clearing is common in all main-sequence stars. Furthermore, the ages of the T Tauri sample in the Mamajek et al. study ($\sim$30 Myr, an order of magnitude or more younger than the nulling sample) implies that debris clearing in the inner system occurs relatively early in the main-sequence lifetime, even in low-mass stars where it is reasonable to believe that radiation pressure forces would be less of a factor than in the A-stars observed with nulling. Thus, one might expect that the stars observed in this study would have no detection of exozodiacal dust. Theoretical models for solar mass stars show that 10 μm excesses peak for stars during terrestrial planet formation, at less than 1 Myr, and then drop off significantly after that, becoming undetectable by current techniques by 10 Myr (Kenyon & Bromley 2004). This result appears to be similar to models of debris around intermediate-mass stars with ages ranging from 10^8 to 10^9 yr, which predict excesses at 10 μm to be a factor of 10^{-2} to 10^{-3} times the stellar photosphere at that wavelength (S. J. Kenyon 2006, private communication). Thus, we find our observations to be consistent with the current models for dust evolution, and previous observational results.

4. NOTES ON INDIVIDUAL OBJECTS

A variety of physical processes alter the distribution of solid matter in main-sequence systems. For debris disks greater than 10^{-3} $M_{\oplus}$ in mass, it is believed that dust destruction is dominated by energetic collisions between grains (Dominik & Decin 2003). Icy grains may also be removed by sublimation, and systems with late-type parent stars and/or a low disk mass may be subject to P–R drag as a dominant removal mechanism (Dominik & Decin 2003). Other dust removal mechanisms which may play important roles in the evolution of debris populations are the presence of a planetary sweeper, photosputtering, or stellar wind drag.

Table 7
Limits on Dust Properties (Using General Opt. Thin Model)

Name	$\langle a \rangle$ (μm)	Mass ($M_{\oplus}$)	f_d
α CrB	9.2	1.5×10^{-5}	1.7×10^{-4}
α Lyr	9.2	2.2×10^{-6}	2.5×10^{-5}
β Leo	4.0	1.2×10^{-6}	6.7×10^{-5}
γ Ser	0.9	5.7×10^{-7}	2.5×10^{-4}
ϵ Eri	0.1	2.4×10^{-7}	4.7×10^{-4}
ζ Lep	3.8	3.4×10^{-6}	2.0×10^{-4}

Reference.
Mamajek et al. (2002).

In this section, we consider three of the objects in our sample which have debris disks which are well studied at longer wavelengths, α Lyr, ϵ Eri, and ζ Lep. For each system, we examine the recent literature and attempt to build a picture of the debris, describing its distribution and likely physical processes occurring in each system.

4.1. Vega (α Lyr)

Vega is one of the closest stellar systems to our own ($d = 8$ pc; Perryman et al. 1997), intrinsically luminous, and has an age well into the main sequence (365 Myr; Rieke et al. 2005). The source null derived for Vega is $0.2 \pm 0.7\%$ (1σ error), consistent with zero, which indicates that we are not detecting resolved emission at our current levels of sensitivity and spatial resolution.

This allows us to place constraints on the distribution and amount of exozodiacal dust surrounding Vega. We are confident (3σ) that there is no resolved emission at 10.6 μm around Vega above the 2.1% level (0.8 Jy) outside of 0.8 AU from the star. The Kelsall model would result in a nulled flux of 1.8 mJy (or 0.0042% of Vega's flux) if placed at the distance of Vega. Scaling up this solar model to our 3σ source null limit for Vega corresponds to a dust density limit of about 220 times our solar system's zodiacal dust. Additionally, we find that the null does not vary significantly with observations at different rotations of the interferometer baseline (over a range of about 90°), indicating that there is no evidence of an inclined disk-like structure.

4.1.1. Physical Interpretation in Light of Spitzer Results

The well studied nature of the debris in the Vega system provides an excellent opportunity to place our 10 μm nulling observations of warm dust in context with dust studies at other wavelengths (hence spatial scales). Recent results from the *Spitzer Space Telescope* have shed light on the distribution of dusty debris in the Vega system, and when viewed together with the nulling results presented here, are illustrative of the power of multiwavelength observations. Su et al. (2005) has found spatially extended emission indicative of cold dust at wavelengths of 24, 70, and 160 μm based upon MIPS observations by the *Spitzer Space Telescope*. The emission is found to be at separations of 300 to 800 AU, with a circularly symmetric and smooth distribution. They have attributed the presence of dust to a large collisional event, followed by a collisional cascade which produces grains smaller than the blowout size. These grains would then be removed by radiation pressure blowout, populating the outer system to large radii. The total dust mass is inferred to be $\sim 10^{-3}$ $M_{\oplus}$. The results of our observations show a relative dearth of material in the inner few AU of the system. The lack of material in the inner system

would seem to support the fact that the vast majority of the grains are collisionally broken down to smaller than blowout size and subsequently pushed outward, a conclusion reached based on MIPS observations by the *Spitzer Space Telescope* (Su et al. 2005).

4.2. ϵ *Eridani*

Far-IR excess was detected by *IRAS* observations at 25, 60, and 100 μm (Backman & Paresce 1993; Backman & Gillett 1987; Aumann 1985), an indication of cold solid material in the circumstellar environment of ϵ Eri. From the observations by Aumann (1985), a disk emitting area of 2.6×10^{-2} AU, or about 5200 Zody was inferred using a simple optically thin ring model. Since these early observations, numerous follow-up observations have been performed at different wavelengths. Greaves et al. (2005) recently observed ϵ Eri at submillimeter wavelengths (450 and 850 μm) and found substantial quantities of dust and substructure in the distribution of the dust at large radii. They find that the cold dust lies in a slightly inclined ring with peak emission at 65 AU (a projected angular separation of about 20″), and an inner cavity. The mass of the ring is significant and estimated to be 5–9 $M_{\oplus}$, and has substantial substructure (i.e., clumpiness). They favor a scenario with a giant planetary perturber at tens of AU. Epsilon Eri has also been the subject of radial velocity planet searches (Cumming et al. 1999; Walker et al. 1995), with a reported detection of a long-period planet in Hatzes et al. (2000). Also characterized by an *Hubble Space Telescope* astrometric study by Benedict et al. (2006), the planet is estimated to have a mass of 1.6 $M_{\rm Jup}$, and a period of about 7 yr, corresponding to a orbital separation of about 3 AU, which is a smaller separation than the planetary perturber predicted by the recent submillimeter observations. Benedict et al. (2006) state that radial velocity data over three decades do show a long period trend consistent with a planetary mass object with a 50–100 yr object, which would be consistent with cold dust observations.

The density of the cold debris in the ϵ Eri system is high enough that one would expect the disk to be collisionally dominated, instead of P–R drag dominated. From this argument, one would not expect dust in the outer system to migrate inward, so the lack of dust in the habitable zone is not surprising. However, another removal mechanism that should be considered is stellar wind (corpuscular) drag, which has a stronger effect than P–R drag for a late-type star. If one adopts the value of 30 $dM_{\odot}/dt$ (Wood et al. 2005) and estimates the timescale for removing grains via stellar wind drag (Chen et al. 2006, Equation 11), one finds that wind drag shortens the removal timescale of the grains by more than a factor of 20. We would then expect the inner system to be populated by grains migrating inward due to stellar wind drag. In this case, the presence of one or more giant planets may also keep the inner system relatively clear of debris.

As this star is lower mass than the other stars in our sample, it is perhaps the best star in our sample to compare to our own solar system. The existence of a giant planet of Jupiter mass at about 3 AU, much like our system, and the existence of cold debris, a Kuiper Belt analog, further warrants comparison to our solar system. The primary debris feature in the inner part of our solar system is the Main Asteroid Belt. The mass of objects in the Main Belt is about 1.8×10^{24} g (Cox 2000) or 3×10^{-4} $M_{\oplus}$. If the derivation of the mass limit for warm debris from our nulling observations was taken to include objects up to 1 km in size, we have an upper limit of about 1×10^{-3} $M_{\oplus}$. Thus, it is conceivable for an asteroid belt-like distribution of debris in the ϵ Eri system to exist below our detection limits, with masses equivalent to our present-day Main Belt asteroids.

4.3. ζ *Leporis*

This object has also been the subject of several studies. Recently, Rieke et al. (2005) found ζ Lep to have one of the largest 24 μm excess in their sample of 76 A-type main-sequence stars, a result which confirms the initial *IRAS* detection (Backman & Paresce 1993). Mid-IR observations with large aperture telescopes have also been made recently by Chen & Jura (2001) on Keck I and Moerchen et al. (2007) with Gemini South. Both studies found, using point-spread function subtraction, that the dust was spatially resolved at about 18 μm but not at 10–12 μm. Various models used to interpret this emission places the longer wavelength emission at less than 9 AU. For the mass of dust grains, Chen & Jura (2001) estimate 1.6×10^{22} g or about 3×10^{-6} $M_{\oplus}$ as a lower limit, assuming an average grain size of 2.8 μm. These results for dusty material at 18 μm are consistent with our nulling observations which find an upper limit in dust mass derived from our 10 μm observations of 1.3×10^{-5} $M_{\oplus}$. Therefore, if some fraction of the dust detected by the previous studies were to migrate inward, it is likely that it would fall below our detection limit. It is important to note that our derived mass is an upper limit, while the mass determined in Chen & Jura (2001) is a lower limit based on their assumption of grain size. A larger assumed grain size would result in a larger mass. Thus, it is a possibility that a greater quantity of dust is present at larger radii than probed by our study.

The SED shape of ζ Lep differs from other Vega-type excess stars, specifically, ζ Lep shows a hotter SED (i.e., a larger excess at around 20 μm compared to 70 and 100 μm). Thus, Rieke et al. (2005) makes the argument that the dust is the result of a recent large collisional event, similar to that hypothesized for the Vega system. Given the spatial scale of the dust emission, the collisional event occurred at a smaller separation (several AU) compared to the Vega event (near 100 AU). The observations point toward a different postcollision scenario in the ζ Lep system as well. If collisional removal of grains was dominant, as in the Vega system, one might expect the long wavelength excesses to be greater than observed. ζ Lep is less luminous than Vega by a factor of about 2 or more, with a blowout grain size about one-third that of Vega. It is conceivable that following the collisional event, fewer grains were subject to blowout, resulting in a lower level of long wavelength excess. If the remainder of the grains were to migrate inward due to P–R drag, one may expect some level excess at shorter wavelengths, perhaps on the same order as detected at 20 μm. Our nulling observations do not rule out this scenario.

5. SUMMARY AND CONCLUSIONS

Our main findings are as follows.

(1) We find no spatially resolved warm debris in these systems with upper limits on warm dust between 400 and 10^4 Zody, depending on the individual objects (see Table 4). This corresponds to dust masses on the order of 10^{-5} to 10^{-6} $M_{\oplus}$.

(2) For all of the objects, these limits contrast with the presence of dust at longer wavelengths (hence greater separations), implying a clearing in dust in the inner system. This suggests that the inner circumstellar environment

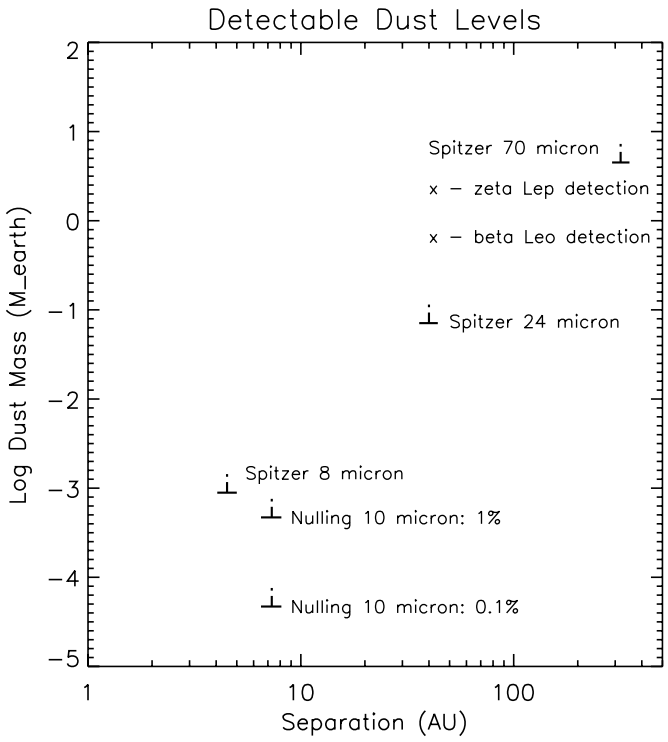

Figure 1. Limits for levels of detectable dust for a range of separations around a hypothetical A-type main-sequence star at 10 pc. Limits are based upon the assumption of purely thermal emission from a population of blackbody grains of a single size, $\sim 15\mu$m. Shown are the limits for photometric detections in three *Spitzer* bands (assuming 5% photometric calibration), as well as nulling interferometric limits for contrast ratios of 100 and 1000. The positive detections for ζ Lep and β Leo by *Spitzer* are indicated by X's. Note that a simplified grain population is used here to illustrate the relative difference in detection levels between observing techniques, and differs from the grain population used for the physical analysis of our observations in Section 3.

around intermediate-mass main-sequence stars are generally cleared of dusty debris. This result is similar to that of Mamajek et al. (2004), who observed a sample of low-mass objects with younger ages.

(3) In the Vega system the primary process keeping dust out of the inner system appears to be a collisional cascade and radiation pressure blowout, a hypothesis suggested by Su et al. (2005). The nulling observations presented in this paper in combination with *Spitzer* MIPS observations at longer wavelengths appear to support this.

(4) In the ϵ Eri system, the lack of material in the inner system is consistent with other evidence for giant planets. This would prevent the large quantities of debris detected at tens of AU from migrating inward due to P–R drag and populating the inner few AU and habitable zone. However, our observations do not rule out a small amount of debris inside the inner giant planet, with a total mass equivalent to our solar system's Main Belt asteroids (present-day mass).

(5) The ζ Lep system may have dust in the 10 μm emitting region consistent with the amount of dust detected at 18 μm (Chen & Jura 2001; Moerchen et al. 2007). Due to the relatively hot SED (larger mid-IR excess versus far-IR excess) compared to other debris disk systems, radiation blowout appears to be less of a factor compared to Vega. This fact is also used by Rieke et al. (2005) to speculate that the system lacks a giant planet. If this is indeed the case, a large collisional event may be responsible for populating the circumstellar environment with dust. Our observations do not rule out the possibility that some fraction of this dust migrated inward and is present in the habitable zone. This make ζ Lep an ideal candidate for follow-up nulling observations once suppression levels are improved.

Future observations should take advantage of the increased sensitivity and longer baselines of telescopes optimized for observations in the mid-IR. Current contrast ratios of about 100 allow us to achieve dust detection levels 2–4 orders of magnitude better than photometric detections at longer wavelengths (with an assumed 5% calibration) for a hypothetical A-type star at 10 pc (Figure 1). Ideally, in future ground-based nulling implementations with AO, we hope to achieve contrast levels of 1000, resulting in another order of magnitude improvement in dust detection levels. Further down the line, the *Large Binocular Telescope*'s large aperture, long baseline, and thermal IR optimized adaptive optics setup (i.e., deformable secondaries) will prove to be a very useful tool in observing debris disks, pushing levels of detectable dust down to a few Zody around nearby stars, or fractional dust luminosities of $\sim 10^{-7}$.

W.M.L. acknowledges support from the Michelson Graduate Fellowship program. We are grateful to the operators and staff at the MMT Observatory for their support of our observations. The authors also thank the referee, Christine Chen, for helpful comments. BLINC was developed under a grant from NASA/JPL. The MMT AO system was developed with support from the Air Force Office of Scientific Research. This work made use of the SIMBAD database.

REFERENCES

Artymowicz, P. 1988, ApJ, 335, L79
Aumann, H. H. 1985, PASP, 97, 885
Backman, D., & Gillett, F. C. 1987, in Proc. Fifth Cambridge Workshop, Cool Stars, Stellar Systems and the Sun, Lecture Notes in Physics, ed. J. L. Linsky & R. E. Stencel (Berlin: Springer), 291, 340
Backman, D. E., & Paresce, F. 1993, in Protostars and Planets III, ed. E. H. Levy & J. I. Lunine (Tucson, AZ: Univ. Arizona Press), 1253
Beichman, C. A., et al. 2005, ApJ, 626, 1061
Benedict, G. F., et al. 2006, AJ, 132, 2206
Bracewell, R. N. 1978, Nature, 274, 780
Brusa, G., et al. 2003, Proc. SPIE, 4839, 691
Chen, C. H., & Jura, M. 2001, ApJ, 560, L171
Chen, C. H., et al. 2006, ApJS, 166, 351
Cox, A. N. 2000, Allen's Astrophysical Quantities (4th ed.; New York: AIP Press)
Cumming, A., Marcy, G. W., & Butler, R. P. 1999, ApJ, 526, 890
Dominik, C., & Decin, G. 2003, ApJ, 598, 626
Greaves, J. S., et al. 2005, ApJ, 619, L187
Greenberg, R., & Nolan, M. C. 1989, Proc. Conf., Asteroids II, ed. M. S. Matthews, R. P. Binzel, & T. Gehrels (Tucson, AZ: Univ. Arizona Press), 778
Grun, E., Zook, H. A., Fechtig, H., & Giese, R. H. 1985, Icarus, 62, 244
Hatzes, A. P., et al. 2000, ApJ, 544, L145
Hinz, P. M., Angel, J. R. P., Hoffmann, W. F., McCarthy, D. W., McGuire, P. C., Cheselka, M., Hora, J. L., & Woolf, N. J. 1998, Nature, 395, 251
Kelsall, T., et al. 1998, ApJ, 508, 44
Kenyon, S. J., & Bromley, B. C. 2004, ApJ, 602, L133
Liu, W. M., Hinz, P. M., Hoffmann, W. F., Brusa, G., Miller, D., & Kenworthy, M. A. 2005, ApJ, 618, L133
Liu, W. M., et al. 2004, ApJ, 610, L125
Mamajek, E. E., Meyer, M. R., Hinz, P. M., Hoffmann, W. F., Cohen, M., & Hora, J. L. 2004, ApJ, 612, 496
Mamajek, E. E., Meyer, M. R., & Liebert, J. 2002, AJ, 124, 1670
Mathis, J. S., Rumpl, W., & Nordsieck, K. H. 1977, ApJ, 217, 425
Moerchen, M. M., Telesco, C. M., Packham, C., & Kehoe, T. J. J. 2007, ApJ, 655, L109
Perryman, M. A. C., et al. 1997, A&A, 323, L49
Rieke, G. H., et al. 2005, ApJ, 620, 1010

Silverstone, M. D. 2000, PhD thesis, Univ. California
Smith, R., Wyatt, M. C., & Dent, W. R. F. 2008, A&A, 485, 897
Spangler, C., Sargent, A. I., Silverstone, M. D., Becklin, E. E., & Zuckerman, B. 2001, ApJ, 555, 932
Su, K. Y. L., et al. 2005, ApJ, 628, 487
Uzpen, B., et al. 2005, ApJ, 629, 512
Walker, G. A. H., Walker, A. R., Irwin, A. W., Larson, A. M., Yang, S. L. S., & Richardson, D. C. 1995, Icarus, 116, 359
Wood, B. E., Müller, H.-R., Zank, G. P., Linsky, J. L., & Redfield, S. 2005, ApJ, 628, L143